JOURNAL OF MATERIALS SCIENCE 32 (1997) 1623–1630

Effect of trivalent cation on the physicochemical properties of cobalt containing anionic clays

S. KANNAN*, C. S. SWAMY
Department of Chemistry, Indian Institute of Technology, Madras-600 036, India

A series of cobalt containing hydrotalcites having the general formula $CoMCO_3$-HT where M = Al, Fe and Cr were synthesized by sequential and coprecipitation methods. The samples were primarily characterized by X-ray diffraction (XRD), infrared absorption studies, transmission electron microscopy-energy dispersive X-ray analysis (TEM-EDAX), thermogravimetry-differential scanning calorimetry (TG-DSC) and BET surface area measurements. The lattice parameters, FTIR stretching wavelengths for O–H bonds and thermal stability depended on the ionic radius of the trivalent M cation. Thermal calcination of these materials yielded a non-stoichiometric spinel-type phase whose crystallinity was also affected by the nature of the trivalent cation.

1. Introduction

Anionic clays, otherwise referred to as hydrotalcite-like (HT-like) compounds are now receiving considerable attention owing to their potential use as adsorbents, ion-exchangers, stabilizers and most importantly as precursors for multicomponent catalysts [1–6]. The structure of these materials can be visualised by starting with a brucite network [$Mg(OH)_2$] in which the Mg occupy the centre of the octahedra of hydroxyl groups that extend through edge sharing thus forming layered sheets and are held by hydrogen bonding. If Mg^{2+} is substituted by a higher valent element (say Al^{3+}), a positive charge density is created in the layer. In order to maintain electroneutrality, anions occupy the interlayer position along with water molecules (which prevent interanionic repulsion) [7]. A schematic representation of brucite and a HT-like network is given in Fig. 1. These materials are normally represented by the general formula $[M(II)_{1-x}M(III)_x(OH)_2]^{x+}[A^{n-}_{x/n}]^{x-}\cdot mH_2O$ wherein M(II) and M(III) are divalent and trivalent cations, A is the gallery anion, x can generally have values between $0.2 < x < 0.4$ and m is normally 4–5. The stabilization of a broad spectrum of divalent and trivalent cations in different atomic compositions with varying interlayer anions in the HT-like network allows the tailoring of desired properties in these materials [8].

The physicochemical properties of these materials are significantly modified by the nature of the divalent ion, trivalent ion and interlayer anion [9, 10]. Clause *et al.* [11] have studied the effect of the trivalent cation (Al and Cr) on the structure and reactivity of Ni-containing HT-like compounds. They concluded that Ni–Cr analogues are poorly crystallized and the oxides generated upon thermal calcination are less stable and readily reducible in comparison with corresponding Ni–Al systems. Recently, Hansen *et al.* [12] have reported a new method for the synthesis of highly crystalline Co–Fe HT-like compounds by aerial oxidation of Fe(II) in a solution of cobalt nitrate. We have earlier reported on the effect of composition on the physicochemical properties of Co–Al HT-like compounds synthesized by coprecipitation under low supersaturation [13]. The present investigation concerns the synthesis and characterization of $CoMCO_3$-HT where M = Al, Fe and Cr with a view to understanding the role of the trivalent cation on the structure, crystallinity and thermal stability of these materials. To our knowledge, this is the first report which emphasises the effect of the trivalent ion on the physicochemical properties of cobalt containing hydrotalcites.

2. Experimental

The HT-like compounds were prepared by sequential precipitation and coprecipitation under low supersaturation using metal nitrate solutions of appropriate concentration and a $NaOH/Na_2CO_3$ mixture (0.2 : 0.15 mol) as precipitants. All the samples were prepared with a Co/M atomic ratio of 3.0. Details of the preparation procedure are given elsewhere [14]. The slurry was aged at 65 °C for 24 h, filtered, washed and dried. The hydrothermal treatment was performed in a teflon lined autoclave at 110 °C for two days under autogenous conditions. Details on the characterization of the samples are discussed elsewhere [13]. The transmission electron microscopic (TEM) studies were carried out in a Philips transmission electron microscope (Model CM12; $h\nu = 120$ kV). The sample was initially dispersed in acetone using an ultrasonic vibrator operating

* Present address: Catalysis Division, National Chemical Laboratory, Pune - 411 008, India

0022–2461

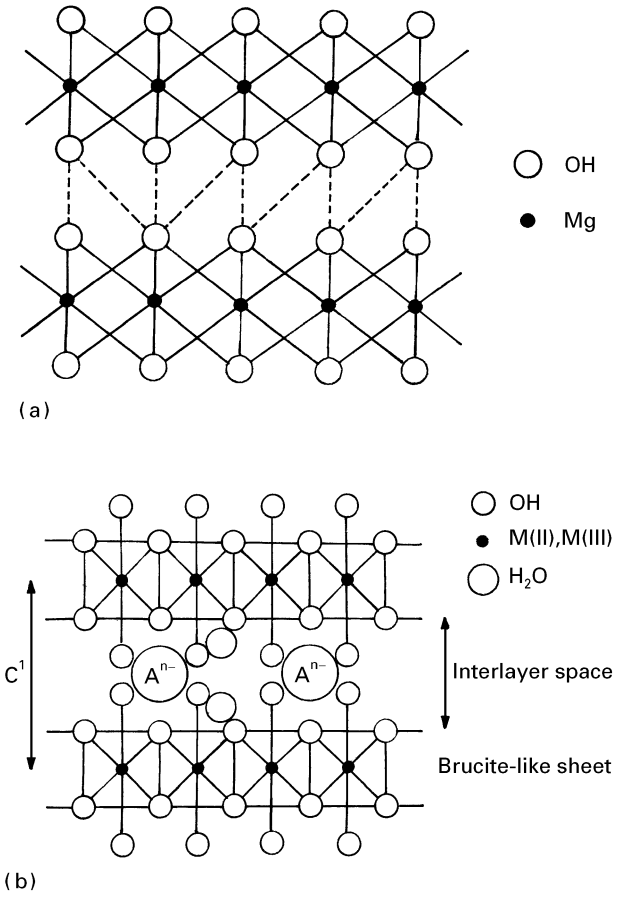

Figure 1 Schematic representation of (a) Brucite and (b) Hydrotalcite.

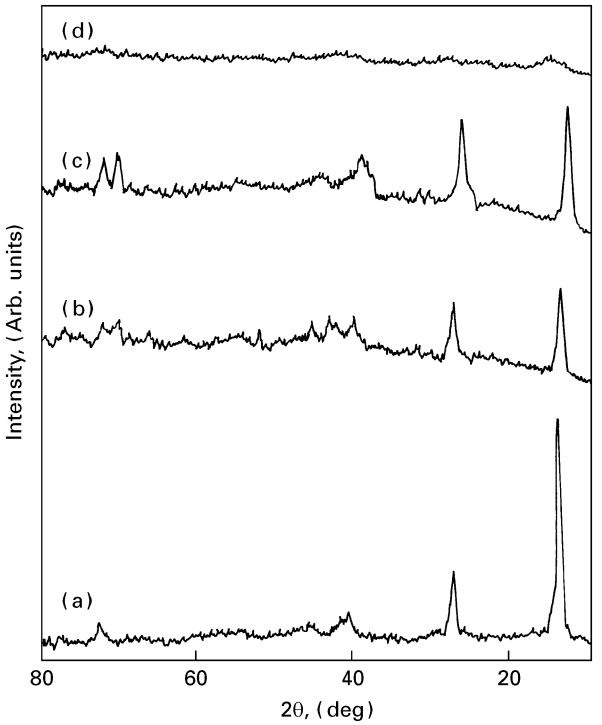

Figure 2 XRD patterns of (a) $CoAlCO_3$-HT (b) $CoFeCO_3$-HT (c) $CoFeCO_3$-HT(LS) (d) $CoCrCO_3$-HT.

at 3 MHz for 1 min. The sample was allowed to settle and a drop of supernatant liquid was placed on a carbon coated copper grid and the solvent was evaporated. The carbon grid was then mounted onto the microscope and micrographs were taken.

3. Results and discussion

Table I furnishes details of the chemical composition, phases obtained, crystallographic parameters and surface area of the samples synthesized. There is no marked difference noticed between the calculated and observed concentration indicating the completion of precipitation. Fig. 2 show the XRD patterns of some of the samples prepared. All the compounds showed a diffraction pattern similar to the pattern of the hydrotalcite-pyroaurite group exhibiting sharp reflections at lower 2θ angles and broad asymmetric reflections at higher diffraction angles. Amongst the samples synthesized, $CoAlCO_3$-HT yielded the maximum crystallinity whereas $CoCrCO_3$-HT showed poor crystallinity. This is inferred from the intensity and symmetry of the nonbasal reflection, which measures the regularity of the stacking of the hydroxide sheets. This is in accordance with the observation obtained for corresponding nickel containing hydrotalcites [11]. The sample prepared under low supersaturation (LS) was a better crystalline material than the corresponding sample prepared under sequential precipitation (SP), obviously due to the slow nucleation and fast crystal growth of the former sample. These results suggest that the crystallinity of the material is considerably modified by the nature of the trivalent cation and the method of preparation. Hydrothermal treatment performed on aged samples enhanced their crystallinity. The crystallite size determined by the X-ray line broadening technique [15] substantiated the above observation indicating an enhancement in the crystallite size upon hydrothermal treatment ($CoAlCO_3$-HT-A = 20 nm and $CoAlCO_3$-HT-H = 22 nm; $CoCrCO_3$-HT-A = 2.6 nm

TABLE I Chemical composition, phase obtained, crystallographic parameters and surface area of the samples synthesized

Compound	M^{2+}/M^{3+} (atomic ratio)	Phase obtained	unit cell parameters		Surface area (m^2g^{-1})
			a (nm)	*c* (nm)	
$CoAlCO_3$-HT-A[a]	3.0	HT[b]	0.3095	2.2751	69.0
$CoAlCO_3$-HT-H	3.0	HT	0.3086	2.2946	43.2
$CoFeCO_3$-HT-A	2.8	HT	0.3129	2.2811	89.3
$CoCrCO_3$-HT-A	2.8	amorphous	–	–	130.1
$CoCrCO_3$-HT-H	2.8	w HT	0.3069	2.1750	132.2
$CoCrCO_3$-HT-A[c]	2.9	w HT	0.3116	2.0501	156.1

(a) $CoAlCO_3$-HT-A is the aged sample and $CoAlCO_3$-HT-H indicate the hydrothermally treated sample (b) Hydrotalcite (c) Prepared under low supersaturation

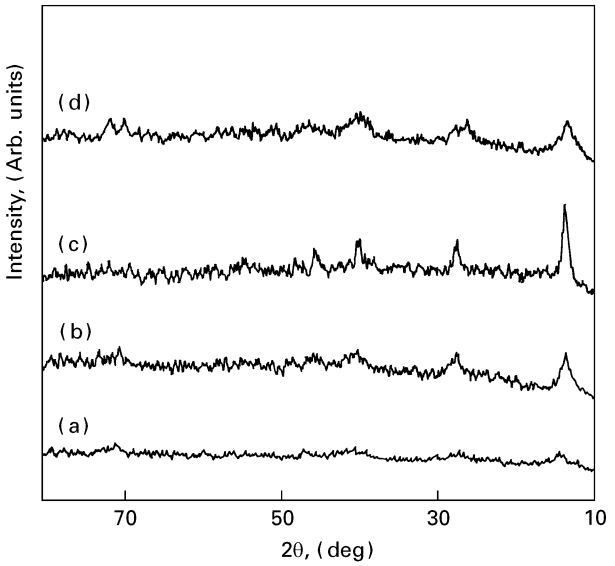

Figure 3 XRD patterns of (a) $CoCrCO_3$-HT-A (b) $CoCrCO_3$-HT-H (110 °C/2d) (c) $CoCrCO_3$-HT-H (110 °C/4d) (d) $CoCrCO_3$-HT(LS).

and $CoCrCO_3$-HT-H = 4.6 nm). It is very clear from these values that the aggregation of particles occurred upon this treatment and lead to an enhancement in the crystallite size. Fig. 3 show the XRD pattern of $CoCrCO_3$-HT subjected to hydrothermal treatment for different time durations. It is clear from this figure, that the crystallinity is enhanced with increasing treatment time. However, the extent of enhancement in the crystallinity upon hydrothermal treatment was different depending on the trivalent cation associated with cobalt. Furthermore, the hydrothermal treatment performed on $CoFeCO_3$-HT showed an amorphous Co–Fe oxide (by XRD) indicating the thermal instability of this material under these conditions, which is similar to the observation of Uzunova *et al.* [16] for Co–Fe hydrotalcites.

The lattice parameters of these samples were calculated by indexing the peaks under an hexagonal crystal system and the differences noticed in their values are in accordance with the ionic radii of the trivalent cation. When a divalent cation in the lattice is replaced by a trivalent cation of smaller ionic radius, there will be a decrease in the unit cell volume and this influences mainly the '*a*' parameter. The higher positive charge due to M^{2+}–M^{3+} substitution is compensated by an interlayer negative charge resulting in electrostatic interaction between the adjacent layers, influencing the '*c*' parameter. Thus the lattice parameters '*a*' and '*c*' increase on going from the Co–Al to the Co–Fe system. The increase in the '*a*' parameter is due to the higher ionic radius of Fe^{3+} (0.065 nm) in comparison with Al^{3+} (0.053 nm) and that for '*c*' is due to reduced electrostatic interaction between layer and interlayer.

Transmission electron microscopy of these materials (Fig. 4) showed well defined hexagonal platelets of thin and wide nature, characteristic of these materials [15]. A closer observation of these particles, at higher magnification, indicated that the surface is pock-marked (microporous nature) which on thermal

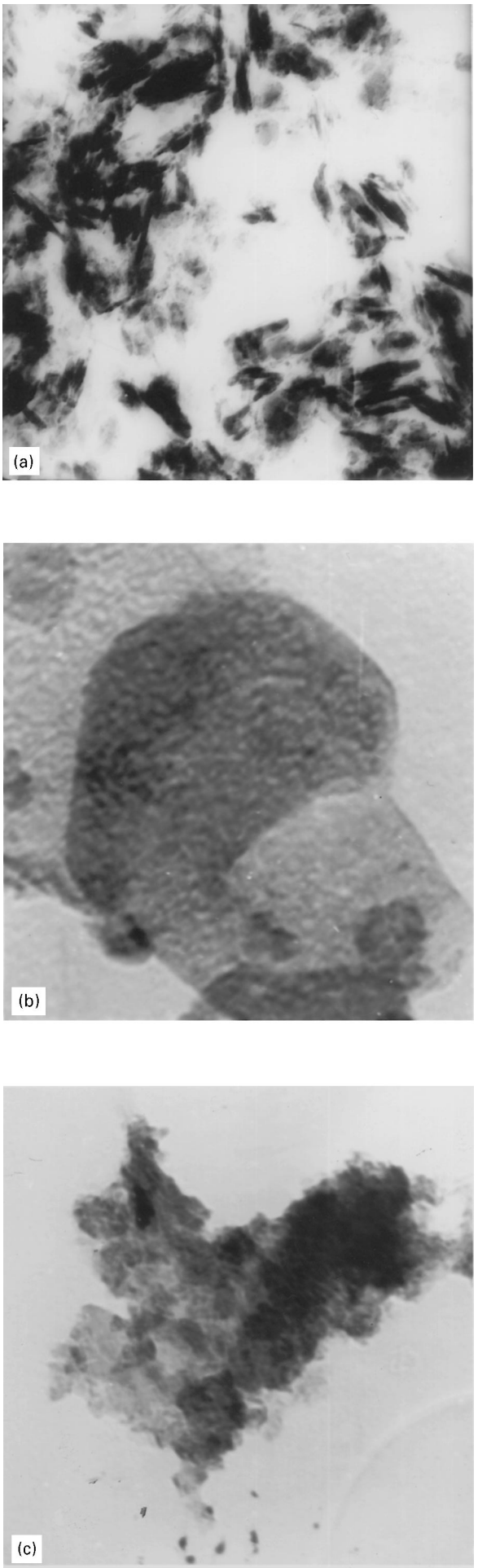

Figure 4 Transmission electron micrograph of (a) $CoAlCO_3$-HT (b) $CoFeCO_3$-HT (c) $CoCrCO_3$-HT.

calcination expand, thus allowing water and CO_2 to exit thereby leading to the formation of mesopores. Calcination of $CoAlCO_3$-HT showed the formation of mesopores with the maximum centred around 4 nm. However, for $CoFeCO_3$-HT, particles with spherical shape were also found along with hexagonal platelets. Comparison of the particle sizes (under the same magnification) indicated that they were smaller for $CoCrCO_3$-HT whereas larger for $CoAlCO_3$-HT, confirming the X-ray results. Another observation noticed on all these samples was the overlapping of the particles even after extensive dispersion indicating a particle-particle interaction. The selective area diffraction (SAD) of these samples indicated a regular hexagonal pattern with well defined crystallographic basal planes corresponding to hydrotalcite. In order to assess the homogeneity of the samples energy dispersive chemical analysis through X-rays (EDAX), was carried out. A typical EDAX pattern of these samples is given in Fig. 5. Different regions with varying spot sizes were chosen to find the atomic composition based on the background subtracted integral intensity of the peaks and the data are summarized in Table II. It is clear from this table that the composition derived at a microscopic level resemble that of the macroscopic level ICPES (Inductively coupled plasma emission spectroscopy) indicating the good homogeneity of the samples. We could not find any discrete particles such as amorphous chromium hydroxy carbonate in the $CoCrCO_3$-HT sample (owing to the poor crystallinity of the sample) indicating that even for this sample a hydrotalcite-like phase is present, however with poor crystallinity.

FT–IR spectra of these samples (Fig. 6) showed prominent bands around 3500, 1630 and 1370 cm^{-1} correspondingly attributed to ν_{OH} stretching, ν_{OH} bending and ν_3 asymmetric stretching of the carbonate thus substantiating the presence of hydroxy carbonate. A closer observation in the ν_{OH} band position indicated a large shift (around 100 cm^{-1}) on varying from one trivalent cation to another. This could be due to the difference in the electron density around the hydroxyl group causing such variation in the band position which, in turn, is affected by the polarisability of the trivalent cation. The band position with proper assignment of some of the samples are summarized in Table III.

The distance between two adjacent layers in a HT-like network c/6 ($\sim$0.3 nm), does not allow coordination of carbonate or water molecules from the interlayer with metal cations in the sheets. Nevertheless, a splitting in the ν_3 vibration of the carbonate was observed along with a weak band around 1030 cm^{-1} attributed to the symmetric valence vibration $\nu_1(A_1)$. The observation of this later band is more prevalent in aged samples. We note that it would be absent if the carbonate ion present in the interlayer possessed the expected D_{3h} symmetry. However, perturbations arising out of the hydrogen bonding between the carbonate ions and the water molecules in the interlayer and hydroxyl groups in the brucite-like sheets result in the lowering of the carbonate symmetry from D_{3h} to C_{3v} or C_{2v} which concomitantly activates the ν_1 vibration of carbonate. Upon hydrothermal treatment of $CoAlCO_3$-HT, ν_1 was completely absent and no splitting in the ν_3 vibration was observed which indicates the enhancement in the ordering of the carbonate anion in the interlayer. However, in the case of Co–Fe and Co–Cr samples, such doublets were

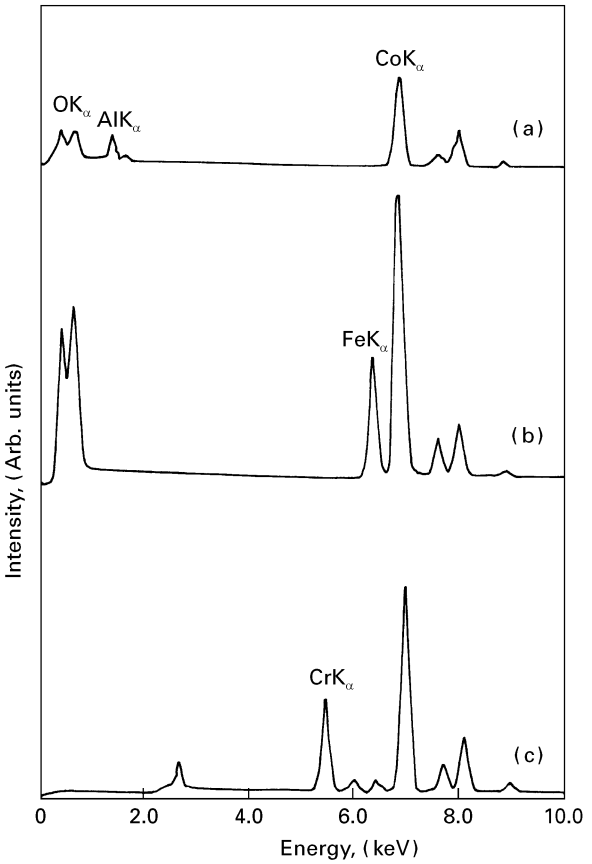

Figure 5 EDAX patterns of (a) $CoAlCO_3$-HT (b) $CoFeCO_3$-HT (c) $CoCrCO_3$-HT.

TABLE II IR band assignments of prepared hydrotalcites

Compound	Hydroxyl vibrations (cm^{-1})		CO_3^{2-} vibrations (cm^{-1})			Lattice vibrations (cm^{-1})
	ν_{OH} (str)	ν_{OH} (bend)	ν_3	ν_2	ν_4	
$CoAlCO_3$-HT-A	3523	1640	1384–1365	880	–	596,549,419
$CoAlCO_3$-HT-H	3479	1640	1365	884	689	595,552,425
$CoFeCO_3$-HT-A	3429	1644	1383–1356	874	–	762,651,566,490
$CoCrCO_3$-HT-A	3443	1629	1383	887	715	570,512,410
$CoCrCO_3$-HT-H	3422	1630	1383–1362	880	718	780,570,512,404

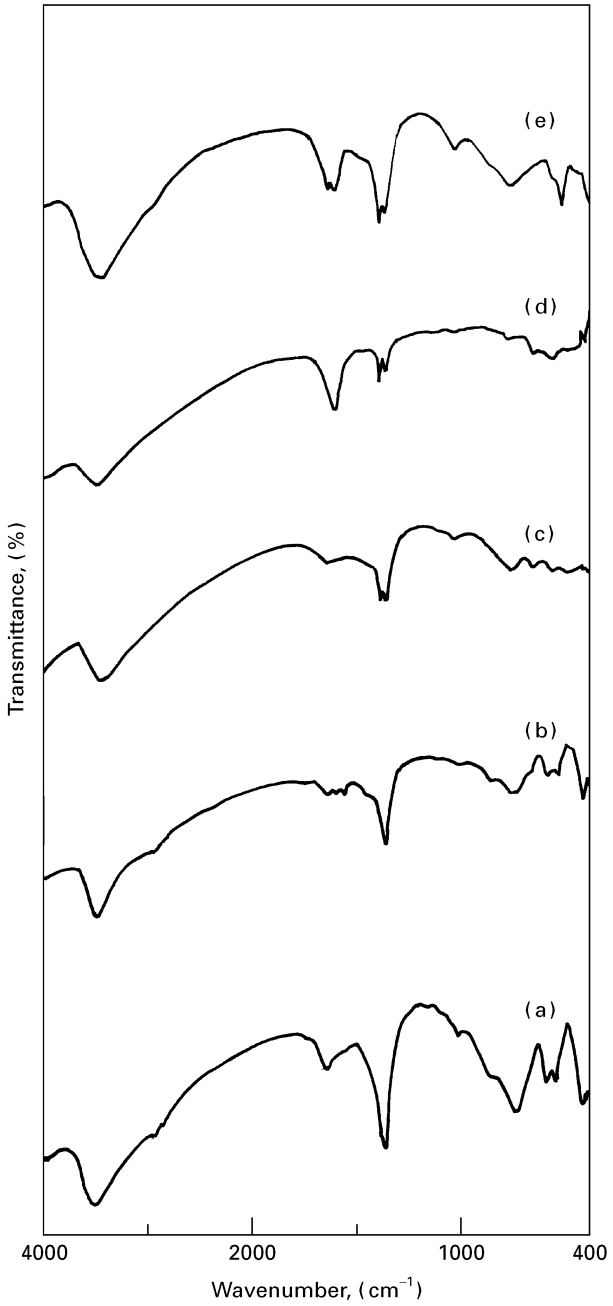

Figure 6 FT–IR spectra of (a) $CoAlCO_3$-HT (b) $CoAlCO_3$-HT-H (c) $CoFeCO_3$-HT (d) $CoFeCO_3$-HT(LS) (e) $CoCrCO_3$-HT(LS).

TABLE III EDAX analysis of some of the synthesized samples

Compound	Spot size	Elem. at.% Co	M	Average Co/M at. ratio
$CoAlCO_3$-HT	7.5	73.2	26.8	2.7
	20	72.8	27.2	
$CoFeCO_3$-HT	25	76.6	23.4	2.8
	25[a]	69.9	30.4	
$CoCrCO_3$-HT	10	74.7	25.3	2.7
	15	70.2	29.7	

[a] Different region

observed for ν_3 carbonate stretching even after hydrothermal treatment which clearly indicates a large degree of disorder for this species in the interlayer. These results could be corroborated with XRD results

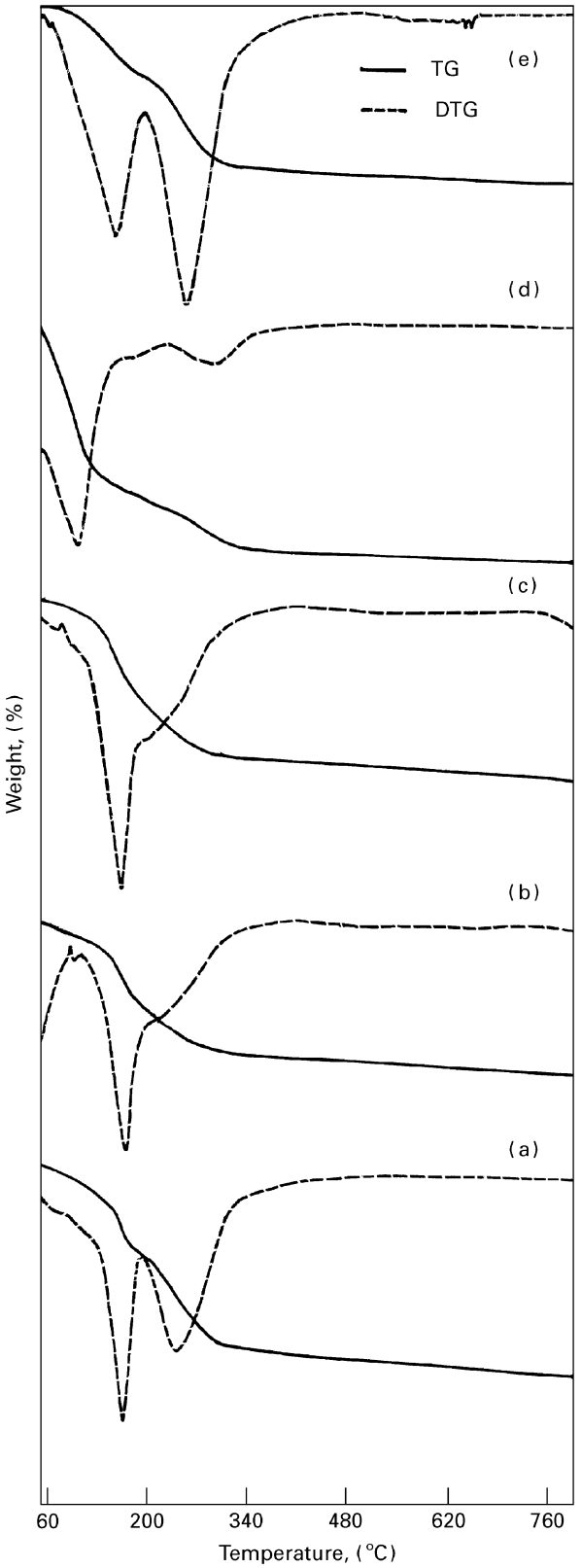

Figure 7 TG–DTG traces of (a) $CoAlCO_3$-HT (b) $CoFeCO_3$-HT (c) $CoFeCO_3$-HT(LS) (d) $CoCrCO_3$-HT (e) $CoCrCO_3$-HT(LS).

which indicated the poor crystallinity of these later samples. A sharp peak was observed around 1600 cm^{-1} for Co–Fe and Co–Cr samples suggesting that it arises not only due to the water bending vibration but also from carbonate ions partially coordinated with metal cations. The observation of such bands are reported for iron (III) hydroxy carbonate and for some other carbonate complexes

TABLE IV TG peak temperature, net weight loss and DSC peak temperature of some of the synthesized samples

Compound	TG peak temperature (°C)		% weight loss	DSC peak temperature (°C)	
	T_1	T_2		T_1	T_2
$CoAlCO_3$-HT-A	171	245	28.7	205	290
$CoAlCO_3$-HT-H	179	232,290	29.2	204	279,318
$CoFeCO_3$-HT-A	167	210	23.3	99	198,242
$CoCrCO_3$-HT-A	101	283	49.8	117	284
$CoCrCO_3$-HT-H	201	288	28.8	218	304
$CoCrCO_3$-HT-A[a]	153	256	26.2	120	194,296
$CoCrCO_3$-HT-H[a]	79	198,299	26.7	106	209,303

(a) Prepared under low supersaturation

[17]. The driving force for the possible presence of such co-ordination could be the large degree of disorder of the carbonate ion possessed by these samples. However, Serna *et al.* [18] have also suggested that the observation of such a band could also be due to the presence of a bicarbonate ion in the interlayer space.

TG analysis, illustrated in Fig. 7, showed, especially for well crystallized samples, two stages of weight loss. The first weight loss ($\sim$12%) is attributed to the elimination of interlayer water and the second one ($\sim$15–20%) is due to dehydroxylation of the brucite-like sheets and decarbonation. However, for less crystalline samples only the second weight loss was observed [Fig. 7c], and in addition this occurred at a lower temperature, while the amount of the first weight loss was considerably reduced. These variations observed in the thermal analysis results seem to be related to the crystallinity of the samples which primarily depends on the method of preparation and the nature of the trivalent cation. DSC results substantiated these TG results in that they exhibit characteristic endotherms corresponding to the weight loss patterns. The DSC thermogram of $CoFeCO_3$-HT showed three stages of transformations, similar to the pattern observed for $NiFeCO_3$-HT by Uzunova *et al.* [19]. The second stage of transformation occurs in two stages involving decarbonation followed by complete dehydroxylation. Some of the hydrothermally treated samples also showed a split in the second transformation, without significantly altering T_1, the peak temperature corresponding to the first transformation. This could be due to better ordering in the interlayer space leading to stepwise weight losses. The TG transformation temperature with net weight loss and DSC peak temperature are summarized in Table IV. It is clear from this table that amongst the trivalent cations studied, Al-containing HT-like compounds are thermally more stable, indicating their strong electrostatic interaction between the layer and the interlayer.

In the case of $CoFeCO_3$-HT, irrespective of the mode of preparation, the release of interlayer water, structural water and CO_2 occurs simultaneously around 170 °C. This suggests that the interaction operating between the sheets and the interlayer anion and water molecules are of similar strength. Furthermore, a better thermal stability is achieved for the samples prepared under low supersaturation than under sequential precipitation, this is especially true for $CoCrCO_3$-HT, which could possibly be due to the better crystallinity of the former samples.

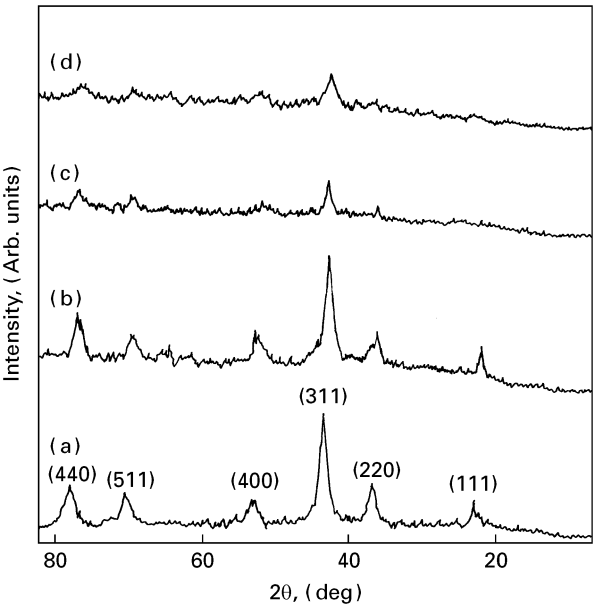

Figure 8 XRD patterns of (a) $CoAlCO_3$-HT (b) $CoFeCO_3$-HT(LS) (c) $CoCrCO_3$-HT (d) $CoCrCO_3$-HT(LS) calcined at 400 °C for 5 h.

TABLE V Lattice parameters and band positions of $CoMCO_3$-HT where M = Al,Fe and Cr calcined at 450 °C for 5 h

Compound	*a* (nm)	IR band position		Surface area ($m^2\,g^{-1}$)
		ν_1	ν_2	
$CoAlCO_3$-HT-A	0.8076	668	567	65
$CoFeCO_3$-HT-A	0.8120	655	565	88
$CoCrCO_3$-HT-A	0.8139	656	560,528	110
Co_3O_4[a]	0.8084	668	596,567	< 5
$CoAl_2O_4$[a]	0.8102	685	558,514	< 5
Co_3O_4[b]	0.8084	672	590	–
$CoAl_2O_4$[b]	0.8103	684	563,523	–
$CoCr_2O_4$[b]	0.8320	630	530	–
$CoFe_2O_4$[b]	0.8390	548	412	–

(a) Ceramic route prepared (b) Samples included for comparison taken from ref. [20]

The results of thermal calcination of some of the compounds at 400 °C for 5 h in air are given in Fig. 8. All the compounds showed a non-stoichiometric

spinel phase irrespective of the trivalent cation. The non-stoichiometry can be explained by the difference in the lattice parameter values and IR band position of the calcined samples compared with that of the stoichiometric compounds, summarized in Table V. The cell parameter and IR band position of Co_3O_4 and $CoAl_2O_4$ prepared through standard ceramic techniques are also included in this table for reference. The lattice parameter values of the calcined catalyst lie between the CoM_2O_4 and Co_3O_4 values indicating the presence of a solid solution. The crystallinity of the spinel strongly depends on the nature of the trivalent cation associated with cobalt. $CoAlCO_3$-CHT showed the highest crystallinity by exhibiting sharp reflections corresponding to the spinel phase whilst $CoCrCO_3$-CHT showed poor crystallinity [compare the (3 1 1) reflections].

Fig. 9 shows the IR spectra of some of the samples calcined at 400 °C for 5 h in air. They show two bands in the region 700–500 cm^{-1}, characteristic of spinels [20]. The band observed around 650 cm^{-1} can be attributed to Co^{2+} in a tetrahedral environment and the band observed around 550 cm^{-1} is due to Co^{3+} in an octahedral environment. A continuous shift in the band position is observed as the elemental composition is changed from CoM_2O_4 (M = Al, Fe and Cr) to $CoCo_2O_4$ indicating the presence of a spinel solid solution arising from the isomorphous M^{3+}/Co^{3+} substitution. A broad band was observed around 1000 cm^{-1} for $CoCrCO_3$-CHT which could due to the presence of a small amount of chromate (due to oxidation of Cr^{3+} to Cr^{6+}) species, which is probably mainly located on the surface.

A closer look at the IR band position would indicate that all the calcined hydrotalcites possess mainly Co_3O_4. This could possibly be due to the large amount of cobalt (~75 at %) present in these samples. This fact is substantiated by Marchi *et al.* [21] who showed the segregation of Co_3O_4 from TPR (temperature programmed desorption) studies for a relatively large concentration of cobalt in Co–Al systems. Furthermore, the variation in the high frequency vibration band on going from one trivalent cation to another is less in comparison with the low frequency vibration band. Since the later band is ascribed for Co^{3+} in O_h symmetry, the possible substitution of the trivalent ion (Al^{3+}, Fe^{3+} and Cr^{3+}) in place of Co^{3+} would alter the nature of the interaction and thereby influencing the band position. The high frequency band was not altered with variation of trivalent cation since it is assigned uniquely to Co^{2+} in t_d symmetry where such substitutional effects do not occur.

An increase in calcination temperature enhanced the crystallinity of the spinel phase (as evidenced from the increase in the intensity and sharpness of the (311) reflection) with concomitant approach in stoichiometry. This result is corroborated with surface area measurements given in Fig. 10 which showed a decrease with increasing calcination temperature. A near one-tenth reduction in the surface area was observed for the sample calcined at 800 °C in comparison with the sample calcined at 200 °C. However, the extent of decrease in the surface area is not significantly affected by the nature of the trivalent cation which is in contrast with the corresponding nickel containing systems [10].

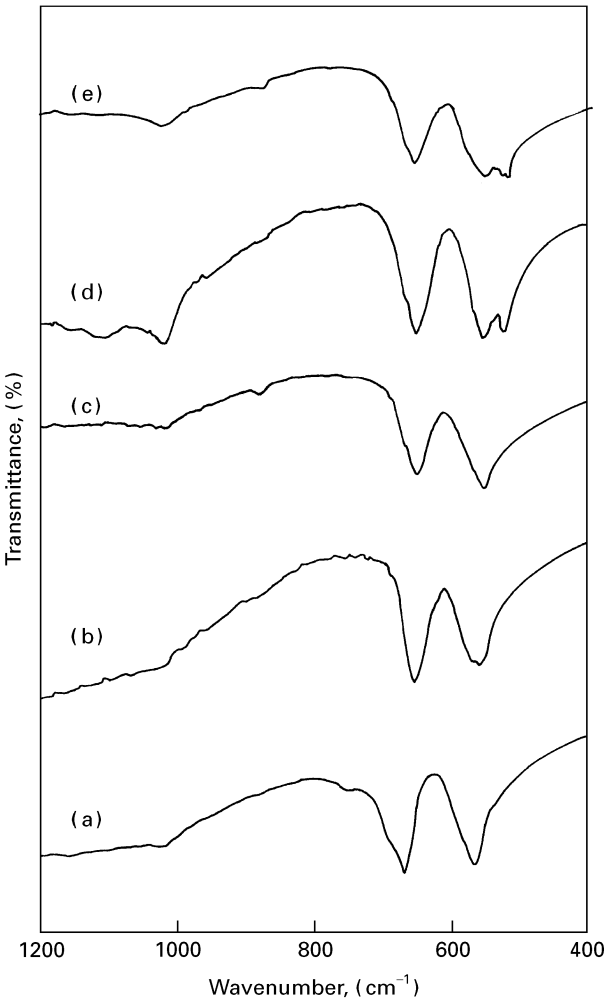

Figure 9 IR spectra of (a) $CoAlCO_3$-HT (b) $CoFeCO_3$-HT (c) $CoFeCO_3$-HT(LS) (d) $CoCrCO_3$-HT (e) $CoCrCO_3$-HT(LS) calcined at 400 °C for 5 h.

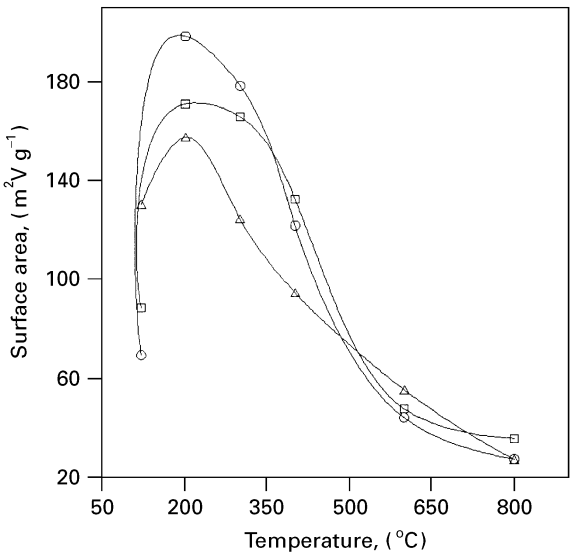

Figure 10 Variation of surface area with calcination temperature of $CoMCO_3$-HT (○) M = Al, (□) M = Cr and (△) M = Fe.

4. Conclusions

(i) The crystallinity, crystallographic parameters, ν_{OH} band position and thermal stability of these materials were affected by the nature, especially the ionic radius, of the trivalent cation. Amongst the trivalent cations studied, aluminium favours a better crystallization of hydrotalcite.

(ii) A good correspondence in the chemical composition was observed between EDAX analysis (microscopic level) and ICPES analysis (macroscopic level) indicating the homogeneity of these samples.

(iii) Calcination of these materials resulted in a non-stoichiometric spinel, irrespective of the trivalent cation, however the physicochemical properties of the spinel depend on the nature of the trivalent cation.

Acknowledgements

The authors thank Air Products Chemicals Inc. for financial assistance. The authors also thank Mrs Kanchanamala of Department of Metallurgy for TEM/EDAX measurements.

References

1. S. MIYATA, *Clays Clay Miner.* **31** (1983) 305.
2. W. T. REICHLE, *CHEMTECH* **16** (1986) 58.
3. A. VACCARI, *La Chimica L'Industria* **74** (1992) 174.
4. C. S. SWAMY, S. KANNAN and S. VELU, in 'Main Group Elements and their Components' (Ed. V. G. Kumar Das) Narosa Publishing House, India (1996) p. 112.
5. S. KANNAN and C. S. SWAMY, *Appl. Catal. B* **3** (1994) 109.
6. S. VELU and C. S. SWAMY, *Appl. Catal.* **119** (1994) 241.
7. R. ALLMANN, *Acta Crystallogr.* **B24** (1968) 972.
8. F. CAVANI, F. TRIFIRO and A. VACCARI, *Catal. Today* **11** (1991) 173.
9. W. T. REICHLE, *J. Catal.* **94** (1985) 547.
10. S. KANNAN and C. S. SWAMY, in Indo-British Seminar on Catalysis in Energy and Environment, Hyderabad, Jan. 30–31 (1995) Abs. p. 30.
11. O. CLAUSE, M. GAZZANO, F. TRIFIRO, A. VACCARI and L. ZOTORSKI, *Appl. Catal.* **73** (1991) 217.
12. H. C. B. HANSEN, C. B. KOCH and R. M. TAYLOR, *J. Solid State Chem.* **113** (1994) 46.
13. S. KANNAN, S. VELU, V. RAMKUMAR and C. S. SWAMY, *J. Mat. Sci.* **30** (1995) 1462.
14. S. KANNAN and C. S. SWAMY, "Preparation of catalysts VI", in "Studies in Surface Science and Catalysis" (vol. 91), Ed. by G. Poncelet, J. Martens, B. Delmon, P. A. Jacobs and P. Grange (Elsevier, Amsterdam, 1995) p. 903.
15. S. KANNAN and C. S. SWAMY, *J. Mat. Sci. Lett.* **11** (1992) 1585.
16. E. UZUNOVA, D. KLISSURSKI, I. MITOV and P. STEFANOV, *Chem. Mater.* **5** (1993) 576.
17. K. NAKAMOTO, in "Infra-red and Raman Spectroscopy of Inorganic and Co-ordination Compounds" (Wiely, New York, 1978) p. 283, 380.
18. C. J. SERNA, J. L. WHITE and S. L. HERN, *J. Pharm. Sci.* **67** (1977) 324.
19. E. UZUNOVA, D. KLISSURSKI and S. KASSABOV, *J. Mater. Chem.* **3** (1993) 121.
20. J. PREUDHOMME and P. TARTE, *Spectrochim. Acta* **27A** (1971) 1817.
21. A. J. MARCHI, J. I. DI COSIMO and C. R. APESTIGUIA, *Catal. Today* **15** (1992) 383.

Received 4 July 1995
and accepted 20 November 1995